Electronic Structure, Porphyrin Core Distortion, and Fluxional Behavior of Bis-Ligated Low-Spin Iron(II) Porphyrinates

ARTICLE *in* THE JOURNAL OF PHYSICAL CHEMISTRY A · JUNE 1997

Impact Factor: 2.69 · DOI: 10.1021/jp963039s

5 AUTHORS, INCLUDING:

F(rances) Ann Walker
The University of Arizona
242 PUBLICATIONS **8,736** CITATIONS
SEE PROFILE

A. X. Trautwein
Universität zu Lübeck
561 PUBLICATIONS **9,822** CITATIONS
SEE PROFILE

Electronic Structure, Porphyrin Core Distortion, and Fluxional Behavior of Bis-Ligated Low-Spin Iron(II) Porphyrinates

Michael Grodzicki,*[1a] Holger Flint,[1a] Heiner Winkler,[1a] F. Ann Walker,[1b] and Alfred X. Trautwein*[1a]

Institut für Physik, Medizinische Universität zu Lübeck, 160 Ratzeburger Allee, 23538 Lübeck, Germany, and Department of Chemistry, University of Arizona, Tucson, Arizona 85721

Received: October 3, 1996; In Final Form: March 24, 1997[⊗]

Three axially bis-ligated Fe(II) porphyrinates, [$PFeL_2$], have been investigated by Mössbauer spectroscopy over the temperature range 4.2−230 K and in an applied field of 6 T. Relatively large differences in the quadrupole splitting ΔE_Q were found among [TMPFe(2-MeImH)$_2$] (**1**), [TMPFe(*N*-MeIm)$_2$] (**2**), and [OEPFe(PMe$_3$)$_2$] (**3**) (1.61, 1.07, and 0.38 mm/s, respectively). Compound **3** exhibits significant line broadening above 150 K that indicates fluxional distortion and/or ligand rotation. Molecular orbital calculations in the local density approximation yield electric field gradients (efg) in good agreement with the measured quadrupole splittings, ΔE_Q, and the measured sign of the efg. The observed differences in quadrupole splittings can be ascribed to distortions (ruffling) of the porphyrin core in **1** as compared to **2** and **3** and to the differences in covalent interactions of the axial nitrogen donors of **1** and **2** and phosphorous donors of **3**. The observed temperature-dependent line broadening of **3** correlates with the low calculated rotational barrier.

Introduction

Model hemes based on iron(II) and iron(III) tetraphenylporphyrinates have found considerable utility in elucidating and understanding the properties of the heme proteins.[2] However, these synthetic hemes often introduce new or different properties that the investigator may not have considered beforehand, for example, rapid rotation of axial ligands in homogeneous solution.[3−8] In comparison to the axial ligands in model hemes, rotation of the axial ligands of heme proteins is precluded because they are linked by side chains that are covalently attached to the protein backbone. The orientations of planar ligands provided by the protein are also tightly controlled by protein structural constraints that include steric crowding of other protein side chains very near the heme and, in the case of histidine ligands, hydrogen-bonding of the NH group of the imidazole ring to either amide carbonyl groups of the protein backbone or, possibly, hydrogen bond acceptors provided as amino acid side chains. Thus, in the heme proteins, there is essentially no possibility of rotation of the axial ligands about the metal−ligand bond.

For the case of heme centers coordinated to two planar imidazole ligands of histidine residues, two limiting orientations of the axial ligand planes have been implicated in the structures of the cytochromes: imidazole planes oriented parallel to each other (cytochromes b_5,[9] three of the heme centers of cytochromes c_3,[10] the *b* hemes of sulfite oxidase[11] and flavocytochrome b_2,[12] and the heme *a* of cytochrome oxidase[13]), while other bis-histidine-coordinated heme proteins are believed to have their axial imidazole planes orientated perpendicular to each other. The latter group has been identified largely on the basis of spectroscopic data for the oxidized (Fe(III)) forms and includes the *b* hemes of mitochondrial complex III, also known as cytochrome bc_1,[14] the similar *b* hemes of cytochrome b_6f of chloroplasts, one of the *c*-type hemes of cytochrome c_3,[10] and the *c*-type heme of cytochrome *c*″ of *Methylophilus methylotrophus*.[15] On the basis of structural and spectroscopic investigation of the bis(2-methylimidazole) complex of tetraphenylporphyrinatoiron(III), [TPPFe(2-MeImH)$_2$]$^+$,[16] we concluded some time ago that for low-spin d^5 ferriheme centers parallel orientation of axial ligands was energetically favored and that either bulky axial ligands, such as 2-methylimidazole (or, as we later found, the combination of 2,6-disubstituted tetraphenylporphyrinates together with pyridines[17,18] or bulky imidazoles[19]), were required to force the perpendicular relative orientation of planar axial ligands in Fe(III) porphyrinates.

During the time over which our studies of bis(hindered imidazole) and bis(pyridine) complexes of Fe(III) porphyrinates were being carried out, we had assumed that for the symmetrical electron configuration of low-spin d^6 Fe(II) porphyrinates planar axial ligands would prefer to align themselves in mutually perpendicular planes, in order to maximize the π-bonding interactions between the d_π orbitals of Fe(II) and those ligands. However, recent investigations have shown that low-spin Fe(II) porphyrinates strongly prefer to have planar axial ligands oriented parallel to each other. These investigations include not only structure determinations by single-crystal X-ray crystallography[20] but also studies of the stability of bis-ligand complexes of Fe(III) and Fe(II) tetraphenylporphyrinates determined by electrochemical methods,[20,21] in which it was shown that only in the presence of bulky 2,6-phenyl substituents is the bis(2-methylimidazole) complex of the Fe(II) porphyrinate stable at ligand concentrations less than 1 M, and even for porphyrinates for which this complex can be formed (tetramesitylporphyrinate, TMP, for example), the stabilities of the bis(2-MeImH) complexes are at least 2 orders of magnitude less than those of the corresponding bis(*N*-MeIm) complexes.[21] The Mössbauer isomer shifts and quadrupole splittings of [TMPFe(2-MeImH)$_2$], [OEPFe(2-MeImH)$_2$], and [TMPFe(1,2-Me$_2$Im)$_2$] measured at 77 K have recently been reported,[22] but no structure of a bis(2-methylimidazole) or related complex of an Fe(II) porphyrinate has yet appeared. However, it is reasonable to expect that, in order to accommodate the bulky 2-methyl groups, the axial ligands must bind in perpendicular planes and the porphyrinate ring must ruffle, as is the case for the Fe(III) analog, [TMPFe(1,2-Me$_2$Im)$_2$]$^+$.[19] In support of this conclusion, we have recently investigated the ^{1}H NOESY/EXSY spectrum of the Fe(II) complex [TMPFe(1,2-Me$_2$Im)$_2$] and shown that it is almost identical to that of [TMPCo(1,2-Me$_2$Im)$_2$]$^+$BF$_4^-$,[8]

[⊗] Abstract published in *Advance ACS Abstracts,* May 1, 1997.

S1089-5639(96)03039-3 CCC: $14.00

suggesting that the structures of the two complexes are very similar. The NOESY and EXSY cross peak patterns observed for $[TMPCo(1,2\text{-}Me_2Im)_2]^+BF_4^-$ are in turn essentially identical (apart from the actual chemical shifts) to those of $[TMPFe(2\text{-}MeImH)_2]^+ClO_4^-$,[5] suggesting that the Co(III) complex has a structure very similar to that of the Fe(III) complex. The rate of rotation of 1,2-Me_2Im on the Fe(II) complex is less than a factor of 10 faster than that on the Fe(III) complex,[3,8] suggesting that the bond lengths and degree of ruffling of the porphyrinate ring are very similar for the two oxidation states.

For electronic structure calculations on systems of the size of $[TMPFe(2\text{-}MeImH)_2]$ (**1**), $[TMPFe(N\text{-}MeIm)_2]$ (**2**), and $[OEPFe(PMe_3)_2]$ (**3**), containing up to 143 atoms and 373 valence orbitals, computational methods based on density functional theory[23−25] offer an attractive alternative to conventional *ab initio* quantum chemical methods because they combine accuracy with modest computational requirements in CPU time and memory space. Even the simpler local density approximation (LDA) yields results for ground-state properties of transition-metal compounds that are generally much better than those obtained in the Hartree−Fock approximation. Accordingly, molecular orbital calculations in LDA by the self-consistent-charge-Xα (SCC-Xα) method[26] have been performed on **1**−**3**, in order to understand the origin of the differences in the spectroscopic data among these three complexes. In particular, we wished to see if these calculations could explain why the bis(2-methylimidazole) complexes of TMPFe(II) and OEPFe(II) and the bis(1,2-dimethylimidazole) complex of TMPFe(II) have such large quadrupole splittings (1.6, 1.7, and 1.7 mm/s, respectively, from measurements at 77 K[22]). For purposes of this study we have focused mainly on tetramesitylporphyrinate complexes, and thus on the bis(2-methylimidazole) complex, $[TMPFe(2\text{-}MeImH)_2]$, **1**. As comparisons, in order to test the reliability of the computational results for **1**, we also calculated the quadrupole splittings of two other complexes, $[TMPFe(1\text{-}MeIm)_2]$, **2**, in which the imidazole ligands are in parallel planes and the porphyrinate ring is nearly planar[27] and for which the quadrupole splitting is typical of that observed for most six-coordinate low-spin Fe(II) porphyrinates having two nitrogen donors (1.0−1.1 mm/s[22]), and the non-physiological complex $[OEP(PMe_3)_2]$, **3**, in which there are no axial ligand planes and for which the quadrupole splitting is very small (0.4 mm/s).[22]

Methods

Mössbauer Spectroscopy. Samples of the bis-ligated Fe(II) porphyrinates $[TMPFe(1,2\text{-}MeIm)_2]$, $[TMPFe(2\text{-}Me_2ImH)_2]$, **1**, $[TMPFe(N\text{-}MeIm)_2]$, **2**, $[OEPFe(PMe_3)_2]$, **3**, and $[TMPFe(PMe_3)_2]$ were prepared previously[22,28] in dimethylacetamide (Aldrich), and their 77 K Mössbauer spectral parameters have been reported.[22] In this work, Mössbauer measurements have been performed on **1**, **2**, and **3** at 4.2 K in a field of 6 T perpendicular to the γ-beam and in zero field between 4.2 and 230 K. Higher temperatures were not feasible because of the low melting point of the solvent (253 K). Measured spectra have been analyzed by a least-squares fit using Lorentzian line shapes. Isomer shifts are given relative to α-Fe at room temperature.

Calculations. Molecular orbital calculations in the local density approximation (LDA) have been performed by the self-consistent-charge-Xα (SCC-Xα) method.[26] Experimentally determined geometries for $[TMPFe(1\text{-}BzlIm)_2]$,[27] which is believed to be an excellent model for **2**, and **3**[28] have been used, apart from the C−H distances that have been enlarged from their "crystallographic" values of 0.93−0.96 Å to typical C−H bond distances in the range 1.06−1.09 Å. For most of the calculations the computationally demanding mesityl groups have been replaced with hydrogen atoms since their influence turned out to be minor even on the barrier for axial ligand rotation. The structural data for **1** are available only for the metal ion being Fe(III)[19] instead of Fe(II). However, following the arguments given in the Introduction, it was assumed that the geometry of the two oxidation states would be quite similar and thus the Fe(III) structural parameters would be representative of those of Fe(II). Again in this case, terminal substituents were replaced with hydrogen atoms in one calculation, but all atoms were included in a second calculation for comparison. The molecular *z*-axis is defined by Fe and its two directly coordinating atoms of the axial ligands. The plane perpendicular to this axis defines the average plane for the porphyrin core. The most important structural parameters are given in Table 3 below, where $|z_{max}|$ denotes the degree of nonplanarity, *i.e.*, the largest deviation of a non-hydrogen porphyrin atom from the average plane. The $Fe-N_{por}$ distance in **1** is about 0.06 Å shorter than in the other two complexes. Since, however, the distance to the axial ligand is almost the same as in **2**, it is likely that this is predominantly a result of the ruffling of the porphyrin ring, which requires that metal−ligand bonds be shortened.[19]

The electric field gradient (efg) tensor has been calculated as described previously.[29] The nuclear quadrupole moment $Q(^{57}Fe) = 0.15$ barn, and the measured quadrupole splitting ΔE_Q is related to the major component V_{zz} of the efg tensor by

$$\Delta E_Q = (1/2)eQV_{zz}(1 + \eta^2/3)^{1/2}$$

with the asymmetry parameter $\eta = |V_{xx} - V_{yy}|/|V_{zz}|$. Core polarization effects are taken into account by the Sternheimer shielding function $\gamma(r)$ derived from atomic self-consistent first-order perturbation calculations.[30] Apart from this approximation the efg is computed rigorously within the frame of a valence-electron-only MO method.

Experimental Results

Representative Mössbauer spectra of **1**, **2**, and **3** recorded at 4.2 K in a 6 T magnetic field applied perpendicular to the γ-beam are shown in Figure 1. The quadrupole splitting varies considerably among these three complexes, as summarized in Table 1. In particular, it is remarkable that **1** reveals a relatively large quadrupole splitting even though the Fe(II) is in the low-spin ($S = 0$) state. Compounds **1** and **2** showed essentially no temperature dependence of the quadrupole splitting or line width of the quadrupole doublet up to 200 K, but **3** showed significant temperature dependence of the line width of the quadrupole doublet above 150 K, as shown in Figure 2. The spectrum of **3** could be fitted by a doublet up to 150 K, whereas for higher temperatures a doublet and a single, rather broad line ($\Gamma \approx 2$ mm/s) were used. Similar behavior has been observed in cases with iron exhibiting cage (bound) diffusion.[31] The line width of the doublet increases between 150 and 222.5 K by about 50%, as summarized in Table 2. Line broadening due to melting of the samples could be detected by measurements on **1** and **2**, which exhibit line broadening only at 230 K. Therefore, line broadening due to melting of **3** could be ruled out. Instead, it can be concluded that fluxional distortion and/or rotation of axial ligands is the reason for the observed line broadening in **3**.

Theoretical Results

Charge Distribution. In spite of the smaller $Fe-N_{por}$ distances in **1** (Table 3), the charge distributions of **1** and **2** are rather similar (*cf.* Table 4), apart from a slightly smaller polarity

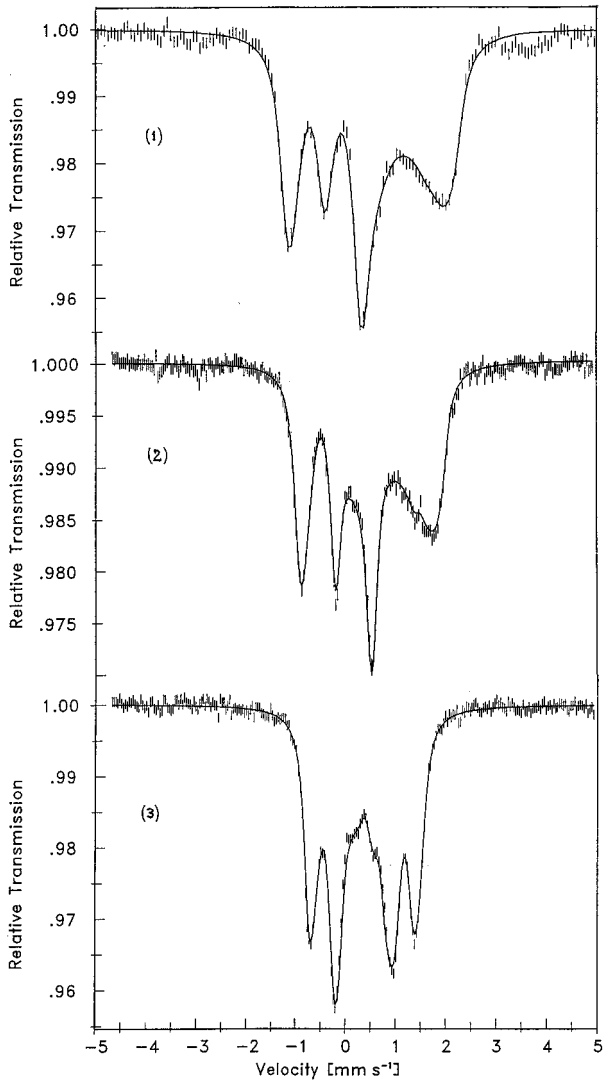

Figure 1. Mössbauer spectra of the low-spin Fe(II) porphyrinates recorded at 4.2 K in a magnetic field of 6 T perpendicular to the γ-beam. Solid lines represent least-squares fits, with results given in Table 1.

TABLE 1: Isomer Shift, δ, Quadrupole Splitting, ΔE_Q, Line Width, Γ (All Values in mm/s), Sign of efg, and Asymmetry Parameter η for the Complexes of This Study[a]

	1	**2**	**3**
δ	0.39(1)	0.45(1)	0.36(1)
ΔE_Q	1.61(1)	1.07(1)	0.38(1)
Γ	0.36(1)	0.26(1)	0.23(1)
sign of efg	>0	>0	>0
η	0.2(1)	0.0(1)	0.6(1)

[a] Data obtained from fits of magnetic Mössbauer spectra recorded at 4.2 K in the presence of a 6 T field applied perpendicular to the γ-beam.

of the Fe bonds in **1** that is reflected in increased overlap populations and in reduced absolute values of the effective charges of Fe, N_{por}, and L_{ax}. The effective charge of Fe in **3** is reduced by approximately a factor of 2 since the axially bonded atom is the positively charged P. The Fe−P bond is considerably more covalent than the axial Fe−N bonds, and the reduced charge of iron leads to a slightly more covalent character of the Fe−N_{por} bond compared with **2**.

Orbital Energies. The ordering of the orbital energies shown in Table 5 is the same in all cases and resembles the splitting pattern of slightly distorted octahedral coordination. The "t_{2g}" manifold of the Fe(3d) orbitals is split into the lower lying d_{xz} and d_{yz}, which are nearly degenerate, and d_{xy}, which is in all

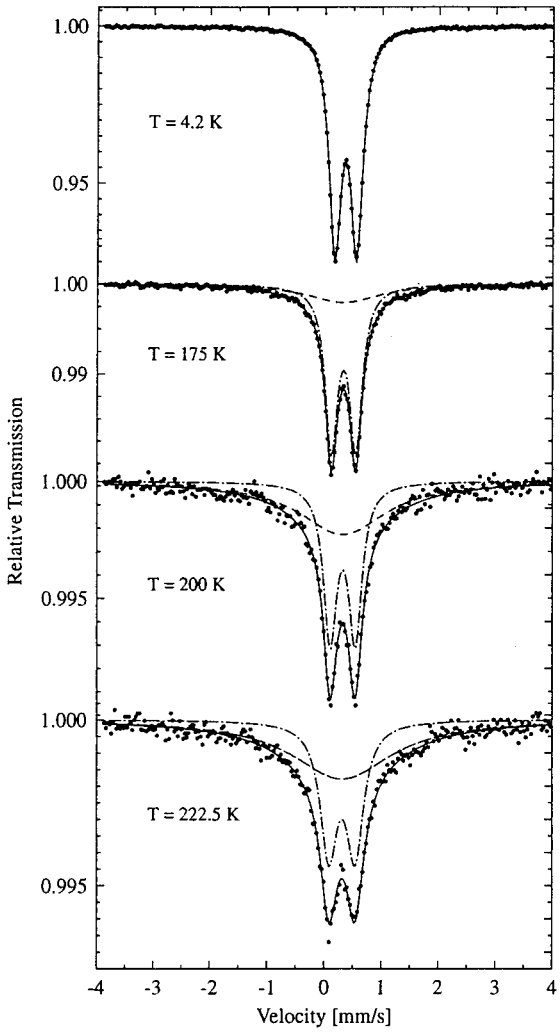

Figure 2. Mössbauer spectra of **3** as a function of temperature.

TABLE 2: Line Width, Γ (in mm/s), for 1, 2, and 3 at Different Temperatures (The Values in Parentheses Refer to the Broad Single Line Observed for 3)

T (K)	**1**	**2**	**3**
77	0.33	0.28	0.25 (−)
150	0.31	0.27	0.24 (−)
200	0.33	0.27	0.28 (1.8)
222.5		0.28	0.37 (2.1)

TABLE 3: Structural Data (Distances in Å)

	1[19]	**2**[27]	**3**[28]
effective symmetry[a]	C_2	D_2	D_4
Fe−N_{por}	1.936	1.992	1.995
Fe−L_{ax}	2.004	2.017	2.275
$\|z_{max}\|$	1.001(C_m)	0.486(C_β)	0.182(C_β)

[a] Effective symmetry of the porphyrinate cation, ignoring the rotational disposition of the methyl groups of PMe_3.

cases slightly higher in energy and thus the HOMO. This is the reverse order of energies of that reported for CO complexes of low-spin Fe(II) porphyrinates[32] and for the low-spin Fe(III) counterparts of all three of these complexes[16,33] (see below for discussion of spin-polarized SCC-Xα calculations), but the same order of orbital energies has been found for other bis(nitrogen base) or (nitrogen base)(thioether) ligations of Fe(II) porphyrinates.[34] Within the empty "e_g" manifold of the octahedral "parent" complexes, d_{z^2} is always below $d_{x^2-y^2}$, but the splitting is considerably smaller with P as axial ligand. In between both manifolds fall the "e_g"-type (in D_{4h} notation) out-of-plane π

TABLE 4: Effective Charges *Q*(A), Overlap Populations *n*(AB), and Valence Shell Occupation n_{nl} of Fe

	1	**2**	**3**
Q(Fe)	+0.551	+0.577	+0.258
$Q(N_{por})$	−0.207	−0.223	−0.212
$Q(L_{ax})$	−0.165	−0.175	+0.484
$n(Fe-N_{por})$	0.320	0.281	0.311
$n(Fe-L_{ax})$	0.251	0.241	0.341
n_{4s}(Fe)	0.35	0.36	0.31
n_{4p}(Fe)	0.56	0.47	0.70
n_{3d}(Fe)	6.54	6.59	6.73

TABLE 5: Orbital Energies, ϵ, in eV, with %Fe(3d) Character in Parentheses

orbital	**1**	**2**	**3**
$d_{x^2-y^2}$	−1.676 (64)	−2.757 (68)	−2.419 (70)
d_{z^2}	−2.259 (69)	−3.080 (71)	−2.460 (55)
Por "$e_g(\pi^*)$"	−3.447 (10)	−3.599 (6)	−3.638 (10)
	−3.454 (9)	−3.767 (7)	−3.663 (10)
d_{xy}	−4.447 (94)	−4.927 (98)	−4.587 (99)
d_{xz}	−4.580 (83)	−4.990 (89)	−4.867 (84)
d_{yz}	−4.586 (83)	−5.008 (86)	−4.870 (84)
Por "$a_{2u}(\pi)$"	−5.985 (3)	−6.074 (−)	−5.864 (−)
Por "$a_{1u}(\pi)$"	−6.184 (3)	−6.360 (−)	−6.469 (−)
Por "$e_g(\pi)$"	−7.605 (2)	−7.844 (2)	−8.103 (2)
	−7.644 (2)	−7.918 (2)	−8.121 (2)
Δ_{cf}[a]	2.188	1.847	2.127
Δ_{ct}[b]	1.126	1.223	1.204
$\lvert a_{2u}-a_{1u}\rvert$	0.259	0.286	0.605

[a] Δ_{cf} is the crystal field energy splitting: $\Delta_{cf} = \epsilon(d_{z^2}) - \epsilon(d_{xy})$. [b] Δ_{ct} is the charge-transfer energy splitting: $\Delta_{ct} = \epsilon(\text{Por "}e_g(\pi^*)\text{"}) - \epsilon(d_{xz})$.

orbitals of the porphyrin (denoted "$e_g(\pi^*)$" in Table 5) that are thus the LUMOs. This result implies a low-energy metal-to-ligand charge-transfer transition (d_{xz},d_{yz} → "$e_g(\pi^*)$") with an energy Δ_{ct} around 1.13 eV (*cf.* Table 5). Such bands are observed in the near-infrared spectra of ferrocytochrome *c*[35] and hemoglobin cyanide.[35]

In comparison, for the oxidized parent Fe(III) species of **1**, the situation is considerably different. A spin-polarized SCC-Xα calculation yields the d_{xy} orbital as the lowest, while the d_{xz}-spin-down orbital is in this case the LUMO, which enables a spin-allowed ligand-to-metal charge-transfer transition from the porphyrin a_{2u} orbital. The corresponding orbital energy difference for this transition is obtained as 0.73 eV or 1700 nm, which is in qualitative agreement with a recently measured MCD spectrum.[36]

The crystal field splitting Δ_{cf} defined as the difference between the orbital energies of $3d_{xy}$ and $3d_{z^2}$ turns out to be large in all cases, *viz.*, larger than 1.8 eV, which confirms the observed low-spin ground state. The decrease of Δ_{cf} from **1** to **2** is connected with the smaller $Fe-N_{por}$ distance in **1**. The larger Δ_{cf} in **3** is caused by the axial ligands PMe_3 since the Fe−P interaction is significantly more covalent than the axial $Fe-N_{Im}$ bonds of the imidazole complexes.

With regard to the degree of splitting between the two components of the filled "$e_g(\pi)$", $d_{xz,yz}$, and empty "$e_g(\pi^*)$" orbitals, not surprisingly, the splitting in each case is much greater for the complex with parallel ligand planes (**2**) than for that with perpendicular planes (**1**). In principle, perpendicular ligand planes should cause no splitting in any of these three orbital sets, but the 1,2-dimethylimidazole ligands bind slightly off-axis due to the bulky 2-methyl group and hence introduce a small rhombic distortion. Moreover, in the case of **2** it is interesting to note that despite the expected "filled−filled" interaction, the splitting of the filled "$e_g(\pi)$" and d_{xz},d_{yz} orbitals (0.074 and 0.018 eV, respectively) is much smaller than that of the empty "$e_g(\pi^*)$" (0.168 eV).

TABLE 6: Calculated and Experimental Quadrupole Splitting (in mm/s), Asymmetry Parameter, and Orientation of the efg

orbital	**1**	**2**	**3**
ΔE_Q(calc)	+1.71	+1.17	+0.43
ΔE_Q(exp)	+1.61	+1.07	+0.38
η(calc)	0.05	0.36	0.09
η(exp)	0.2	0.0	0.6
$\hat{q}$	$\hat{z}$	$\hat{z}$	$\hat{z}$

TABLE 7: Fe Valence Shell Occupation Numbers, p and d Shell Anisotropies, and efg Contributions in mm/s

	1	**1A**	**1B**	**1C**	**2**	**3**
n_{4px}(Fe)	0.208	0.175	0.193	0.206	0.172	0.229
n_{4py}(Fe)	0.205	0.167	0.191	0.206	0.163	0.230
n_{4pz}(Fe)	0.151	0.150	0.151	0.154	0.138	0.243
n_{3dxy}(Fe)	1.982	1.987	1.984	1.989	1.988	1.990
n_{3dxz}(Fe)	1.740	1.842	1.764	1.804	1.859	1.767
n_{3dyz}(Fe)	1.756	1.801	1.779	1.802	1.805	1.766
n_{3dz^2}(Fe)	0.479	0.452	0.472	0.448	0.438	0.750
$n_{3dx^2-y^2}$(Fe)	0.584	0.494	0.554	0.535	0.500	0.457
Δn_p	+0.056	+0.022	+0.042	+0.052	-0.014	−0.014
Δn_d	+0.339	+0.206	+0.295	+0.273	+0.219	−0.070
V_{zz}^{TD}(p)	+0.264	+0.104	+0.177	+0.244	+0.140	−0.063
V_{zz}^{TD}(d)	+1.274	+0.770	+1.106	+1.021	+0.818	−0.257
V_{zz}^{val}	+1.36	+0.85	+1.20	+1.11	+0.89	−0.15
V_{zz}^{cov}	+0.18	+0.05	+0.12	+0.17	+0.08	−0.03
V_{zz}^{lig}	+0.15	+0.16	+0.15	+0.17	+0.17	+0.58

Finally, in all systems the porphyrin a_{1u}-like orbital lies below the a_{2u}-like orbital. However, in the case of PMe_3 as axial ligands the difference in energy is distinctly larger than for imidazole. A similar trend is observed for cysteine as axial ligand.[37,38] It may be concluded that a_{1u} will be stabilized with respect to a_{2u} for axial ligands with heavier ($Z \geq 11$) atoms.

Electric Field Gradients. The calculated quadrupole splittings are positive in all cases, η is small, and the direction $\hat{q}$ of the electric field gradient (efg) is almost identical with the molecular *z*-axis. For this reason, the discussion can be restricted to the V_{zz} components of the efg. Moreover, since η is small, these may be decomposed into three contributions, which are denoted as valence, covalency, and ligand contributions.[29] (These three contributions add up to the total V_{zz} only if η exactly equals zero.) It is seen from Table 6 that the quadrupole splitting in **1** and **2** is dominated by the valence contribution, which is roughly proportional to the anisotropy $\Delta n_d = n(d_{x^2-y^2}) + n(d_{xy}) - n(d_{z^2}) - [n(d_{xz}) + n(d_{yz})]/2$ of the Fe(3d) shell occupation. The covalency contribution arising from the Fe−ligand overlap populations is more than twice as large in **1** as in **2**, again due to the shorter $Fe-N_{por}$ distance in **1**. Finally, the ligand contribution to V_{zz} arising from the ion cores and the valence electrons of all ligand atoms makes only a small and almost negligible part of the total efg. In **3** the situation is completely different. The quadrupole splitting is dominated by the ligand contribution, whereas the valence part even has the opposite sign but in any case is very small.

Discussion

Electric Field Gradients. The difference between the quadrupole splittings of **1** and **2** and the large value of the former are the most intriguing questions in view of the similarity of the axial ligands. Since in both complexes the efg is dominated by the valence contribution, this difference is expected to be related to the anisotropy of the valence shell occupation Δn_d and, to a minor extent, Δn_p. In fact, Δn_d turns out to be about 50% larger in **1** than in **2**, and a more detailed analysis (*cf.* Table 7) shows that this difference arises mainly from an increase of $n(3d_{x^2-y^2})$ in **1** and a simultaneous decrease of

$n(3d_{xz,yz})$, so that the slightly larger $n(3d_{z^2})$ of **1** cannot reverse the trend to a larger efg. This is in accordance with the differences in the respective charge distributions, as Fe in **1** exhibits stronger covalent bonding to the porphyrin than **2**, whereas the axial ligands apparently cannot be thought to be responsible for the efg differences.

This conclusion is supported by an additional calculation on a model system ("**1A**", also summarized in Table 7) by combining the porphyrinato core of **2** with the axial ligands of **1**. The resulting value for the total efg is 1.13 mm/s with $\eta = 0.29$, both values being close to the corresponding values of **2**. Moreover, the details of the p and d shell occupation are almost identical for **2** and **1A** so that the p shell anisotropy also cannot account for the differences between **1** and **2**. This is elucidated by computing the 3d and 4p contributions to V_{zz} separately in the Townes−Dailey (TD) approximation.[39] In both cases $V_{zz}^{TD}(p)$ is nearly the same and about 15% of the corresponding $V_{zz}^{TD}(d)$ values (*cf.* Table 7).

It could be argued that the stronger covalent bonding, together with the larger anisotropy Δn_d found for **1** than **2**, is just due to the shorter Fe−N_{por} bond lengths in the former than in the latter. The question then arises, have we prejudiced the case by assuming the Fe−N_{por} bonds to be shorter for **1** than they actually are because we have, as described in the Methods section, used the structural parameters for the Fe(III) analog, $[TMPFe(1,2\text{-}Me_2Im)_2]^+$,[19] for the calculations summarized in Tables 4−7? However, there are several indications that the short bond lengths observed for $[TMPFe(1,2\text{-}Me_2Im)_2]^+$ [19] are predominantly a result of the ruffling of the porphyrin ring, which requires that metal−ligand bonds be shortened, as discussed previously,[19] and that in fact the Fe(III) and Fe(II) complexes should have very similar structures, with similar ruffling of the porphyrinato core and similar Fe−N_{por} bond lengths. First, the bond lengths of Fe(II) porphyrinates bound to nonhindered imidazoles are, on average, only 0.005 Å longer than their Fe(III) analogs[20] (parallel ligand planes in both cases). Furthermore, for bis-pyridine-ligated porphyrinates, where the pyridine ligand planes are aligned parallel in the Fe(II) complexes but perpendicular in the Fe(III) complexes, the bond lengths of the Fe(II) porphyrinates are, on average, 0.025 Å longer than their (ruffled) Fe(III) counterparts. Comparing nonhindered imidazole complexes (parallel axial ligand planes) of Fe(III) to those of hindered imidazole complexes (perpendicular axial ligand planes), the 2-MeImH complex has Fe−N_{por} bonds that are 0.022 Å shorter[40] than those of a variety of ImH complexes,[20] and $[TMPFe(1,2\text{-}Me_2Im)_2]^+$ (perpendicular planes), which is much more highly ruffled[19] than the 2-MeImH complex, has Fe−N_{por} bonds that are 0.052 Å shorter than those of $[TMPFe(1\text{-}MeIm)_2]^+$ [17] (parallel planes). Finally, our recent NOESY/EXSY results[8] provide very strong evidence that the structures of $[TMPFe(1,2\text{-}Me_2Im)_2]^+$ and its Fe(II) analog are extremely similar, and the similar rates of axial ligand rotation for the two oxidation states also suggest that the Fe−N_{por} bond lengths are very similar. All of these facts together support the view that the shortening of the Fe−N_{por} bond is due to ruffling of the porphyrinate ring rather than to a significant intrinsic Fe−N_{por} bond length difference between Fe(II) and Fe(III). Nevertheless, assuming that there may be such an intrinsic difference in Fe−N_{por} bond lengths of the two oxidation states of up to 0.025 Å (as in the pyridine complexes discussed above), we have done two additional series of model calculations for **1**, where (i) the Fe−N_{por} bond is taken as 1.961 Å, an increase of 0.025 Å over that observed for its Fe(III) analog[19] (labeled as "**1B**" in Table 7), and (ii) the porphyrin core is made planar while all distances are kept the same as in **1** (labeled as "**1C**" in Table 7). The positions of the axial ligands were maintained the same in these calculations.

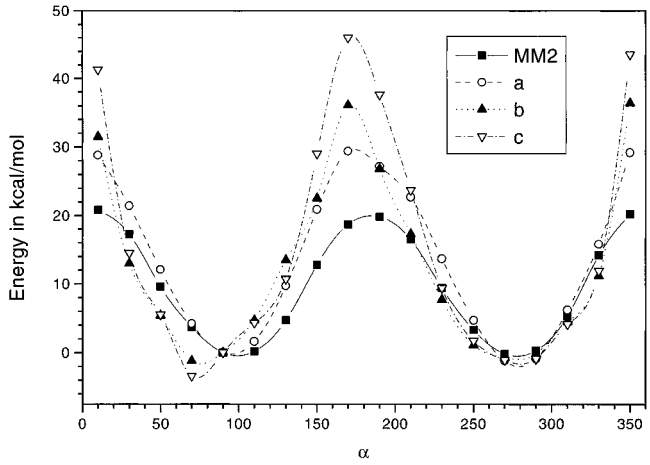

Figure 3. Rotational barriers for **1** computed by a molecular mechanics method (MM2),[6] and in local density approximation for Fe(III) without mesityl groups (a), for Fe(II) without mesityl groups (b), and for Fe(II) with mesityl groups (c). All values are in kcal/mol and relative to the configuration with the two axial ligand planes perpendicular to each other ($\alpha = 90°$).

The calculated quadrupole splittings are reduced by 0.24 mm/s for (i) and by 0.25 mm/s for (ii). The reason for this reduction in both cases can be described as arising mainly from a decrease in covalent bonding between Fe and the porphyrin core, which weakens both the π interaction of $Fe(3d_{xz,yz})$ and the σ interaction of $Fe(3d_{x^2-y^2})$ with the corresponding $N_{por}(2p_\pi)$ and $N_{por}(2p_\sigma)$ orbitals. Accordingly, the $Fe(3d_{xz,yz})$ orbitals contribute less to the empty antibonding e_g-type orbitals so that the corresponding occupation numbers, $n(3d_{xz})$, $n(3d_{yz})$ become slightly larger. Conversely, the $Fe(3d_{x^2-y^2})$ orbital mixes less into the low-lying, doubly occupied σ-bonding molecular orbital, and the occupation number $n(3d_{x^2-y^2})$ decreases. The two changes together yield a reduction of the Fe(3d) shell anisotropy of 0.044 for (i) and of 0.066 for (ii), so that the change is more pronounced for the transition to planarity (with the bond distances kept constant) than for enlarging the Fe−N_{por} distance by 0.025 Å, whereas the covalency contribution to V_{zz} is more affected for (i). All together, these model calculations demonstrate that it is the ruffling of the porphyrin core that leads to the large observed quadrupole splittings in two ways, *viz.*, (a) directly by increasing the covalency of the bonding interaction between Fe and the porphyrin core, and (b) indirectly, by the decrease of the Fe−N_{por} bond distances, which itself again yields stronger covalent interactions.

In summary, according to the theoretical results, the difference in the electric field gradients and in the observed quadrupole splittings in **1** and **2** arises mainly from differences in the d shell occupations of Fe, which themselves are caused predominantly by ruffling of the porphyrin core of **1**, but not by the identity of the axial ligands. Therefore, the influence of the axial ligands on iron has to be described in these two cases as indirect, since they lead to different distortions of the porphyrin core, which then cause the differences in the observed quadrupole splittings. On the other hand, the axial ligands PMe_3 in **3** directly influence the electronic structure of iron because they lead, first, to a substantially enhanced $n(3d_{z^2})$ occupation within the e_g subshell of Fe(3d) due to strong covalent σ-bonding between $Fe(3d_{z^2})$ and $P(3p_z)$ and, second, to a somewhat more anisotropic ligand field, which in this case dominates the efg.

Rotational Barriers. An explanation for the difference in the temperature dependence of the line widths among the three

complexes can be given by comparing the rotational barriers for axial ligand rotation. In a first series of model calculations the porphyrin core and one ligand are kept fixed while the other ligand is rotated in steps of 15° around the *z*-axis. An upper limit for the height of the barrier may then be derived from the variation of the total energy as a function of the rotation angle α. This procedure yields values for the barriers of 130 kcal/mol for complex **1**, 10.6 kcal/mol for **2**, and of 1.7 kcal/mol for **3**. Whereas it is clear that in the first two cases rotation of the axial ligands is inhibited in the measured temperature range, the small barrier for complex **3** may be accessible at elevated temperature. However, these results can be considered only as qualitative, first of all, because the porphyrin core has been kept rigid. In particular, the high barrier for **1** clearly indicates that the porphyrin will change its structure upon axial ligand rotation. Therefore, a second series of calculations has been performed on **1** with geometries derived from molecular mechanics simulations.[6] The plane of one axial ligand is fixed at an angle of 40° with respect to an Fe−N_{por} bond, while the other ligand is rotated in steps of 20° around the *z*-axis. The angle between the two planes will be denoted by α. The geometry of the porphyrin core is then optimized for each of these configurations of the axial ligands by doing molecular mechanics (MM2) minimization of each of these structures.[6,41] The optimized geometries are then utilized to perform density functional electronic structure calculations for the three subsequent cases: (a) the cationic complex with Fe(III) without the mesityl groups; (b) the neutral system containing Fe(II) without the mesityl groups; and (c) the neutral system containing Fe(II) with the mesityl groups.

The results of these three calculations, which are summarized in Figure 3, where they are also compared to energy barriers calculated by MM2 techniques for the Fe(III) analog,[6] indicate, as expected, a distinct reduction of the barrier from 130 kcal/mol to about 36 kcal/mol for the comparable case b. Next, and more importantly, it can be seen that the mesityl groups exhibit some influence on the height of the barrier, but without changing the qualitative shape, hence justifying the omission of the mesityl groups in the majority of the MO calculations. Finally, replacing Fe(II) with Fe(III) yields minima of the binding energy for the two orthogonal orientations of the axial ligand planes, in qualitative accordance with the outcome from the molecular mechanics calculations.[6] Taking into account this decrease of the barrier for **1** with a flexible porphyrin ring, the barrier of **3** must be very small, which is consistent with the observation of dynamic behavior of **3** (Figure 2) due to fluxional distortion and/or rotation of the axial ligands.

Acknowledgment. Support of this research by the Deutsche Forschungsgemeinschaft (A.X.T.) and the U.S. National Institutes of Health Grant DK 31038 (F.A.W.) is gratefully acknowledged. The authors wish to thank Konstantin I. Momot for providing the coordinates obtained from the MM2 energy minimizations for the calculations of the energy barriers of **1** that are reported in Figure 3.

References and Notes

(1) (a) Medizinische Universitat zu Lübeck. (b) University of Arizona.
(2) Walker, F. A.; Simonis, U. Iron-Porphyrin Chemistry. In *Encyclopedia of Inorganic Chemistry*; Berliner, L. J., Reuben, J., Eds.; Plenum: NY, 1993; pp 133−274.
(3) Nakamura, M.; Groves, J. T. *Tetrahedron* **1988**, *44*, 3225.
(4) Walker, F. A.; Simonis, U. *J. Am. Chem. Soc.* **1991**, *113*, 8652.
(5) Shokhirev, N. V.; Shokhireva, T. Kh.; Polam, J. R.; Watson, C. T.; Raffii, K.; Simonis, U.; Walker, F. A. *J. Phys. Chem.* **1997**, *A101*, 2778.
(6) Momot, K. I.; Walker, F. A. *J. Phys. Chem.* **1997**, *A101*, 2787.
(7) Nakamura, M.; Tajima, K.; Tada, K.; Ishizu, K.; Nakamura, N. *Inorg. Chim. Acta* **1994**, *224*, 113.
(8) Polam, J. R.; Shokhireva, T. Kh.; Raffii, K.; Simonis, U.; Walker, F. A. *Inorg. Chim. Acta*, in press.
(9) Mathews, F. S.; Czerwinski, E. W.; Argos, P. In *The Porphyrins*; Dolphin, D., Ed.; Academic Press: New York, 1979; Vol. VII, p 108.
(10) (a) Pierrot, M.; Haser, R.; Frey, M.; Payan, F.; Astier, J.-P. *J. Biol. Chem.* **1982**, *257*, 14341. (b) Higuchi, Y.; Kusunoki, M.; Matsuura, Y.; Yasuoka, N.; Kakudo, M. *J. Mol. Biol.* **1984**, *172*, 109.
(11) Kipke, C. A.; Cusanovich, M. A.; Tollin, G.; Sunde, R. A.; Enemark, J. H. *Biochemistry* **1988**, *27*, 2918.
(12) (a) Xia, Z.-X.; Shamala, N.; Bethge, P. H.; Lim, L. W.; Bellamy, H. D.; Xuong, N. H.; Lederer, F.; Mathews, F. S. *Proc. Natl. Acad. Sci. U.S.A.* **1987**, *84*, 2629. (b) Dubois, J.; Chapman, S. K.; Mathews, F. S.; Reid, G. A.; Lederer, F. *Biochemistry* **1990**, *29*, 6393.
(13) Iwata, S.; Ostermeier, C.; Ludwig, B.; Michel, H. *Nature* **1995**, *376*, 660.
(14) (a) Salerno, J. C. *J. Biol. Chem.* **1984**, *259*, 2331. (b) Tsai, A.; Palmer, G. *Biochim. Biophys. Acta* **1982**, *681*, 484. (c) Tsai, A.-H.; Palmer, G. *Biochim. Biophys. Acta* **1983**, *722*, 349.
(15) (a) Berry, M. J.; George, S. J.; Thomson, A. J.; Santos, H.; Turner, D. L. *Biochem. J.* **1990**, *270*, 413. (b) Costa, H. S.; Santos, H.; Turner, D. L.; Xavier, A. V. *Eur. J. Biochem.* **1992**, *208*, 427. (c) Costa, H. S.; Santos, H.; Turner, D. L. *E. J. Biochem.* **1993**, *215*, 817.
(16) Walker, F. A.; Huynh, B. H.; Scheidt, W. R.; Osvath, S. R. *J. Am. Chem. Soc.* **1986**, *108*, 5288.
(17) Safo, M. K.; Gupta, G. P.; Walker, F. A.; Scheidt, W. R. *J. Am. Chem. Soc.* **1991**, *113*, 5497.
(18) Safo, M. K.; Gupta, G. P.; Watson, C. T.; Simonis, U.; Walker, F. A.; Scheidt, W. R. *J. Am. Chem. Soc.* **1992**, *114*, 7066.
(19) Munro, O. Q.; Marques, H. M.; Debrunner, P. G.; Mohanrao, K.; Scheidt, W. R. *J. Am. Chem. Soc.* **1995**, *117*, 935.
(20) Safo, M. K.; Nesset, M. J. M.; Walker, F. A.; Debrunner P. B.; Scheidt, W. R. To be submitted to *J. Am. Chem. Soc.*
(21) Nesset, M. J. M.; Shokhirev, N. V.; Enemark, P. D.; Jacobson, S. E.; Walker, F. A. *Inorg. Chem.* **1996**, *35*, 5188.
(22) Polam, J. R.; Wright, J. L.; Christensen, K. A.; Walker, F. A.; Flint, H.; Winkler, H.; Grodzicki, M.; Trautwein, A. X. *J. Am. Chem. Soc.* **1996**, *118*, 5272.
(23) Parr, R. G.; Yang, W. *Density Functional Theory of Atoms and Molecules*; Oxford University Press: New York, 1989.
(24) Dahl, J. P., Avery, J., Eds. *Local Density Approximations in Quantum Chemistry and Solid State Physics*; Plenum Press: New York and London, 1984.
(25) Labanowski, J. K., Andzelm, J. W., Eds. *Density Functional Theory Approaches to Chemistry*; Springer-Verlag: New York, 1991.
(26) Grodzicki, M. *J. Phys. B* **1980**, *13*, 2683.
(27) Safo, M. K.; Scheidt, W. R.; Gupta, G. P. *Inorg. Chem.* **1990**, *29*, 626.
(28) Mink, L. M.; Polam, J. R.; Christensen, K. A.; Bruck, M. A.; Walker, F. A. *J. Am. Chem. Soc.* **1995**, *117*, 9329.
(29) Grodzicki, M.; Männing, V.; Trautwein, A. X.; Friedt, J. M. *J. Phys. B* **1987**, *20*, 5595.
(30) Lauer, S.; Marathe, V. R.; Trautwein, A. X. *Phys. Rev.* **1979**, *A19*, 1852.
(31) Planchinda, A. S.; Sedov, V. E.; Khromov, V. I.; Suzdalev, I. P.; Goldonskii, V. I.; Nienhaus, G. V.; Parak, F. *Phys. Rev.* **1992**, *B45*, 7716.
(32) Case, D. H.; Huynh, B. H.; Karplus, M. *J. Am. Chem. Soc.* **1979**, *101*, 4433.
(33) Walker, F. A.; Simonis, U. Proton NMR Spectroscopy of Model Hemes. In *Biological Magnetic Resonance, Vol. 12: NMR of Paramagnetic Molecules*; Berliner, L. J., Reuben, J., Eds; Plenum: New York, 1993; Table 10.
(34) Makinen, M. W.; Churg, A. K. Structural and Analytical Aspects of the Electronic Spectra of Hemeproteins. In *Iron Porphyrins, Part One*; Lever, A. B. P., Gray, H. B., Eds.; Addison Wesley: Reading, MA, 1983; pp 141−235.
(35) Churg, A. K.; Makinen, M. W. *J. Chem. Phys.* **1978**, *68*, 1913; Erratum, *J. Chem. Phys.* **1978**, *69*, 2268.
(36) Cheesman, M. R.; Walker, F. A. *J. Am. Chem. Soc.* **1996**, *118*, 7373.
(37) Zakharieva, O.; Grodzicki, M.; Trautwein, A. X.; Veeger, C.; Rietjens, I. M. C. M. *J. Biol. Inorg. Chem.* **1996**, *1*, 192.
(38) Antony, J.; Grodzicki, M.; Trautwein, A. X. *J. Phys. Chem.* **1997**, *A101*, 2692.
(39) Townes, C. H.; Dailey, B. P. *J. Chem. Phys.* **1949**, *17*, 782.
(40) Scheidt, W. R.; Kirner, J. L.; Hoard, J. L.; Reed, C. A. *J. Am. Chem. Soc.* **1987**, *109*, 1963.
(41) The authors are grateful to Konstantin I. Momot for performing these MM2 calculations.